AD-A118 789 CHICAGO UNIV IL JAMES FRANCK INST F/G 20/8
ROTATIONALLY MEDIATED SELECTIVE ADSORPTION AS A PROBE OF ISOTRO--ETC(U)
AUG 82 C YU, C S HOGG, J P COWIN, K B WHALEY N00014-77-C-0240
UNCLASSIFIED TR-2 NL

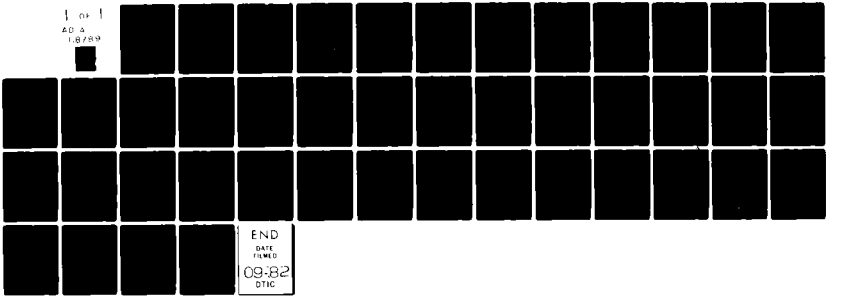

(12)

OFFICE OF NAVAL RESEARCH
Contract N00014-77-C-0240.P00005
Task No. NR-392-023
TECHNICAL REPORT NO. 2

ROTATIONALLY MEDIATED SELECTIVE ADSORPTION AS A PROBE OF ISOTROPIC AND ANISOTROPIC MOLECULE - SURFACE INTERACTION POTENTIALS: HD(J)/Ag(111)

by

Chien-fan Yu, Charles S. Hogg, James P. Cowin†, K. Birgitta Whaley
John C. Light and Steven J. Sibener

Prepared for Publication

in

Israel Journal of Chemistry

Department of Chemistry
and James Franck Institute
The University of Chicago
5640 South Ellis
Chicago, IL 60637, USA

August, 1982

†Present Address: Department of Chemistry, University of Toronto,
Toronto, Ontario, Canada

SECURITY CLASSIFICATION OF THIS PAGE (When Data Entered)

REPORT DOCUMENTATION PAGE

READ INSTRUCTIONS BEFORE COMPLETING FORM

1. REPORT NUMBER: 2	2. GOVT ACCESSION NO.: AD-A118789
3. RECIPIENT'S CATALOG NUMBER:	
4. TITLE (and Subtitle): ROTATIONALLY MEDIATED SELECTIVE ADSORPTION AS A PROBE OF ISOTROPIC AND ANISOTROPIC MOLECULE-SURFACE INTERACTION POTENTIALS: HD(J)/Ag(111)	5. TYPE OF REPORT & PERIOD COVERED: Interim Technical Report
	6. PERFORMING ORG. REPORT NUMBER:
7. AUTHOR(s): Chien-Fan Yu, Charles S. Hogg, James P. Cowin, K. Birgitta Whaley, John C. Light, and Steven J. Sibener	8. CONTRACT OR GRANT NUMBER(s): N00014-77-C-0240.P00005
9. PERFORMING ORGANIZATION NAME AND ADDRESS: University of Chicago, 5801 South Ellis, Chicago, IL 60637	10. PROGRAM ELEMENT, PROJECT, TASK AREA & WORK UNIT NUMBERS: NR-392-023
11. CONTROLLING OFFICE NAME AND ADDRESS: Office of Naval Research, 800 North Quincy Street (Code 613C:CD), Arlington, Virginia 22217	12. REPORT DATE: August, 1982
	13. NUMBER OF PAGES: 39
14. MONITORING AGENCY NAME & ADDRESS (if different from Controlling Office): Office of Naval Research, Physics Program Code 421, 800 North Quincy Street, Arlington, Virginia 22217	15. SECURITY CLASS. (of this report): Unclassified
	15a. DECLASSIFICATION/DOWNGRADING SCHEDULE:

16. DISTRIBUTION STATEMENT (of this Report)

This document has been approved for public release and sale; its distribution is unlimited.

17. DISTRIBUTION STATEMENT (of the abstract entered in Block 20, if different from Report)

18. SUPPLEMENTARY NOTES

Submitted as an invited contribution to the Israel Journal of Chemistry, August, 1982.

19. KEY WORDS (Continue on reverse side if necessary and identify by block number)

Selective Adsorption; Rotationally Mediated Selective Adsorption, Bound State Resonances, Rotationally Inelastic Gas-Surface Scattering, Gas-Surface Interaction Potentials, Physisorption, R-Matrix Calculations.

(Sub 2) beta P sub 2 theta)

20. ABSTRACT (Continue on reverse side if necessary and identify by block number)

Rotationally mediated selective adsorption scattering resonances are used to make an experimental and theoretical study of the laterally averaged interaction potential between HD and a weakly corrugated system, Ag(111). The experimentally observed resonances determine the vibrational levels of the HD/Ag(111) physisorption potential as a function of bound rotational state. These vibrational levels show J-dependent shifts due to the orientational anisotropy of the potential. Exact quantum scattering calculations using a full laterally averaged potential of the form $V_o(z,\theta) = V_o(z) [1 + \beta P_2(\cos\theta)]$ have been carried out

DD FORM 1 JAN 73 1473

Unclassified

SECURITY CLASSIFICATION OF THIS PAGE (When Data Entered)

to obtain rotationally inelastic transition probabilities. Experimental and theoretical resonance energies are compared for two forms of $v_o(z)$, a Morse and a variable exponent potential, as a function of β, and are found to be very close to the first order perturbed energies of a free rotor in bound states of $v_o(z)$. Both potential forms give equally good fits to the data, yielding an optimum value of the asymmetry parameter, $\beta \approx -0.05$. The determination of β is relatively insensitive to small changes in the $v_o(z)$ well depth.

Unclassified

ROTATIONALLY MEDIATED SELECTIVE ADSORPTION AS A PROBE OF ISOTROPIC AND ANISOTROPIC MOLECULE - SURFACE INTERACTION POTENTIALS: HD (J)/Ag(111)

Chien-fan Yu, Charles S. Hogg, James P. Cowin†, K. Birgitta Whaley, John C. Light and Steven J. Sibener

Department of Chemistry
and James Franck Institute
The University of Chicago
5640 South Ellis
Chicago, IL 60637, USA

Submitted as an invited contribution to the Israel Journal of Chemistry.

†Present address: Department of Chemistry, University of Toronto, Toronto, Ontario, Canada

PACS: 79.20,Rf; 34.50. Ez; 34.20.-b; 34.10.+x.

ABSTRACT

Rotationally mediated selective adsorption scattering resonances are used to make an experimental and theoretical study of the laterally averaged interaction potential between HD and a weakly corrugated system, Ag(111). The experimentally observed resonances determine the vibrational levels of the HD/Ag(111) physisorption potential as a function of bound rotational state. These vibrational levels show J-dependent shifts due to the orientational anisotropy of the potential. Exact quantum scattering calculations using a full laterally averaged potential of the form

$$V_0(z,\theta) = v_0(z) \left[1 + \beta P_2(\cos\theta)\right]$$

have been carried out to obtain rotationally inelastic transition probabilities. Experimental and theoretical resonance energies are compared for two forms of $v_0(z)$, a Morse and a variable exponent potential, as a function of β, and are found to be very close to the first order perturbed energies of a free rotor in bound states of $v_0(z)$. Both potential forms give equally good fits to the data, yielding an optimum value of the asymmetry parameter, $\beta \simeq -0.05$. The determination of β is relatively insensitive to small changes in the $v_0(z)$ well depth.

I. INTRODUCTION

The scattering of atomic and molecular beams from well-characterized single crystal surfaces is attracting considerable experimental and theoretical interest at this time [1,2]. One of the primary objectives of these studies is to determine the nature of the interaction potentials which exist between a wide variety of incident atomic and molecular particles and different classes of clean or adsorbate covered crystalline surfaces including, for example, metals, alkali halides, semiconductors, graphite and rare gases. Knowledge of these gas-surface potentials is central to our understanding of many important heterogeneous processes since they determine the dynamics and energetics, i.e.,the time evolution of these phenomena on the molecular level. In addition, very accurate information on surface electron charge density distributions and surface structures can also be extracted from diffraction experiments, provided that the electrostatic terms contributing to the overall gas-surface potential are known. For helium-surface interactions a theoretical framework which analytically relates surface electron charge densities to the helium-surface potential is now in hand[3,4], and has been used in conjunction with first principles surface charge density calculations to obtain structural information from diffraction data[5].

Recent attention in this field has been focused on the study of interaction potentials between helium, atomic hydrogen, molecular hydrogen, and several highly corrugated clean surfaces,[1,2] and physisorbed layers of xenon on graphite[6,7] and silver[8]. One of the primary reasons for studying these particular systems is the large non-specular diffraction peaks which they show. Consequently, very strong diffractive selective adsorption scattering resonances can be observed for these systems. Such diffractive

selective adsorption resonances, which were first observed in 1930 by Estermann and Stern[9] and subsequently explained by Lennard-Jones and Devonshire,[10] are extremely useful as they can be used to determine the eigenvalues of the laterally averaged particle-surface interaction potential. The resulting eigenvalue spectrum can then be used to determine the shape (but not absolute location) of the laterally averaged potential with respect to the surface plane, by either fitting the spectrum to that of a model potential, or by a procedure analogous to a Rydberg-Klein-Rees (RKR) potential inversion[11-14]. In some special instances splittings are observed when two diffractive selective adsorption resonances are mixed by the periodic part of the gas-surface potential. When this occurs information on the higher Fourier coefficients of the periodic potential expansion can be also be obtained from analysis of the band structure of the resonances[15].

In our laboratory we are currently attempting to extend the above studies to include the detailed aspects of *molecular* interactions with relatively smooth metallic surfaces. Several scattering experiments and complementary close-coupled scattering calculations have now been carried out in order to quantitatively determine both the *isotropic* and *anisotropic* (orientation dependent) components of the laterally averaged molecular hydrogen - Ag(111) potential. The experimental studies include determination of the bound physisorption levels of HD on silver as a function of rotor state, using our newly developed technique of rotationally mediated selective adsorption (hereafter, RMSA)[16]; determination of the physisorption levels for H_2 and D_2 on silver using diffractive selective adsorption (hereafter, DSA) scattering resonances; and determination of the rotationally inelastic scattering cross-sections as a function of collision energy for H_2, D_2 and

HD reflecting from silver.

The motivation for making the above measurements is quite straightforward. The isotropic "zeroth-order" physisorption potential can best be determined by mapping out the J=0 bound state resonances for H_2 and D_2 using DSA. Once this is determined, DSA measurements for J=1 H_2 and D_2, and RMSA measurements for HD(J>0) can be used to obtain the anisotropic component of the molecule-surface potential. The basis for this is that the anisotropy of the laterally averaged potential gives rise to J and m dependent shifts of the observed bound state eigenvalues. For both DSA and RMSA measurements the eigenvalue spectrum is given by first order perturbation theory[17]. Analysis shows that DSA measurements are dependent upon both the J and m states of the bound rotor, whereas RMSA measurements on a weakly corrugated surface show J-dependence only, since m is conserved for a flat surface. (The incident HD ensemble used in these studies was predominantly in the $|J,m\rangle = |0,0\rangle$ state). An estimate of the anisotropic component can then be arrived at by comparing the experimental resonance energies with those obtained from the close-coupled calculations. The rotationally inelastic H_2 and D_2 cross-sections are also quite sensitive to the anisotropy of the interaction and will utimately be used as an independent test of the potential derived from the RMSA and DSA studies.

In this paper we present one aspect of this comprehensive study, namely the experimental and theoretical results for the RMSA studies of HD interacting with Ag(111) as a function of bound rotational state. A brief review of the RMSA process is presented in the results section of the paper. This work follows our earlier study of HD/Pt(111) interactions[16] and our subsequent demonstration that Wigner (L^2) R-matrix scattering techniques can be used to investigate the nature of molecule-surface bound states[17]. Similar quantum calculations have also been recently reported by Schinke[18]

who treated the rotational degree of freedom exactly within the diffraction sudden approximation[19]. We feel that Ag(111) is a nearly ideal surface for these studies due to its inert chemical properties with respect to molecular hydrogen. This has allowed us to cryogenically cool the substrate in order to diminish the diffuse inelastic component and Debye-Waller attenuation of the scattered molecules, relative to that which was achieved with Pt(111).

It should be emphasized that the RMSA results presented in this paper have been used to determine the anisotropic component of the hydrogen/Ag(111) potential by building upon the "zeroth-order" isotropic potential which was recently obtained in our DSA studies of H_2 and D_2 on Ag(111)[20]. It is our belief that the unique and complementary information obtained by combining RMSA and DSA measurements will enable the determination of hydrogen/surface interaction potentials for a wide variety of substrate materials.

II. APPARATUS AND EXPERIMENTAL PROCEDURE

The scattering apparatus used in these studies can be schematically portrayed as consisting of four main sections which are the beam source and vacuum manifold, detector, crystal assembly and associated surface analysis equipment, and data acquisition electronics. Each of these sections will be briefly reviewed before describing our experimental procedures. A detailed description of the apparatus has been presented previously[21].

The HD needed for these experiments was generated catalytically by passing an 8:1 H_2: D_2 mixture through a 600 K stainless steel column which was packed with magnesium granules. The HD generator is operated on-line, and has worked reliably for well over one year. The H_2: D_2 ratio was chosen

to be 8:1 in order to make the best compromise between producing a beam of relatively low velocity dispersion and high HD intensity. The isotopically equilibrated effluent of this column (nominally 4:1 H_2: HD) is passed through an in-line liquid nitrogen cooled molecular sieve trap which serves to remove any moisture coming from the HD generator or from the feed gas itself. This trap was necessary as most of the experimental data was collected with the crystal held at cryogenic temperatures. The beam source contained a 20 micron pinhole and could be ohmically heated or cryogenically cooled with liquid nitrogen. Three different beam energies were used: E_b=40.6 meV (P_N = 150 PSI, $\Delta v/v$ = 5.0% FWHM), E_b=113.6 meV (P_N = 250 PSI, $\Delta v/v$ = 5.2%) and E_b=153.0 meV (P_N = 300 PSI, $\Delta v/v$ = 6.0%). An electroformed skimmer was used to ensure a high terminal Mach number for the HD expansion[22].

The nozzle beam is differentially pumped in three stages in a non-bakeable source chamber, with typical operating pressure being $5X10^{-3}$, $1X10^{-5}$, and $5x10^{-7}$ torr for the regions before the skimmer, before the beam collimator, and containing the chopper, respectively. The main UHV scattering chamber is separated from the three source chamber regions by a bakeable buffer region whose pressure rises to $5x10^{-9}$ torr when the beam is on. This buffer section is separated from the chopper section by a sliding gate valve which contains the 0.5mm diam. beam defining aperture. Supported by a 400 l/sec ion pump and a titanium sublimation pump, the crystal chamber has a base pressure of $\sim 7x10^{-11}$ torr, which rises as high as $1x10^{-9}$ torr when the beam is on. The incident beam is collimated to an angular divergence of 0.1°, which corresponds to a 0.5mm diam. beam spot at the crystal.

Particle detection is accomplished with a doubly differentially pumped quadruple mass spectrometer, which rotates about a horizontal axis in the

plane containing the incident beam and the surface normal. The electron bombardment ionizer is located 14.45 cm from the sample, and is collimated to view the crystal with 1.2^{o} resolution. The detector can be rotated manually or under computer control.

The Ag(111) crystal was cut from a 99.999% boule and polished at the Cornell Materials Preparation Laboratory. It was subsequently re-polished in our laboratory with very fine cerium oxide. This was followed by electro-chemical etching with a saturated chromic acid-10% HCl solution[23]. The residue from this treatment was removed with a 10% HNO_3 solution. The orientation of the crystal was checked by Laue X-ray back reflection and was found to be within $\leq \frac{1}{2}^{o}$ of the (111) plane. The underside of the crystal disc was spotwelded to two 1mm thick Pt wires, which were attached through two tungsten rods to the manipulator. A Chromel-Alumel thermocouple was also spotwelded to the back of the crystal. The crystal can be resistively heated or conductively cooled through the Pt support wires. Temperature regulation is achieved with a home built circuit which controls the current source. The crystal can be translated in three mutually perpendicular directions, tilted out of plane, and rotated about two orthogonal axes to set its azimuthal and polar orientation with respect to the incident beam.

After bakeout, the crystal was subjected to several cycles of Ar ion sputtering (2 μamps at 500 V for 10 minutes) until no appreciable contamination could be detected with a single-pass CMA Auger spectrometer. The crystal was then annealed at 600 K for one hour to remove sputter damage. The success of this annealing procedure was verified by the fairly uniform He and H_2 reflectivities which were measured along several points of the crystal. Debye-Waller corrected reflectivities (i.e., extrapolated to T_S = 0 K) of 85% were observed for H_2 incident at $\theta_i = 70^{o}$, 50^{o}, and 30^{o} with respect to

the surface normal.

Data acquisition and instrument control is carried out with a PDP11 minicomputer which is interfaced to the scattering apparatus *via* CAMAC. Time-of-flight measurements are made with a 255 channel multiscaler which has a minimum dwell time of 0.25 μsec/channel. Molecular beam gating is carried out with a 15.24 cm diam. chopper which contains two narrow slots for velocity analysis (0.5 mm width) and two 50% duty cycle patterns for angular distribution measurements. Angular distributions are obtained with two 32 bit scalers which are synchronized to the chopper in order to collect signal plus background (slot open) and background only (slot closed) information. RMSA signals were collected by a Keithley electrometer, demodulated by a lock-in amplifier, passed to a digital voltmeter, and finally read into the computer.

In the next section two types of experimental data are presented: an HD angular distribution and several RMSA scans. Each experiment was always preceeded and immediately followed by a beam characterizing time-of-flight measurement. The angular distribution was obtained by scanning the detector in 0.2^{o} increments for fixed orientation of the crystal with respect to the incident beam. The RMSA scans were taken by measuring the maximum intensity of each outgoing rotationally elastic or inelastic diffraction peak as a function of incident angle. In practice, data was collected for only one diffraction peak at a time as θ_i was varied. This allowed us to alternately move the crystal polar angle by ca. 0.2^{o}, and then scan the detector through the same peak with the computer determining the angle of peak reflected intensity by recording in real time the signal intensity versus detector angle. The peak heights determined in this manner include contributions from both the coherently scattered particles and the diffuse inelastic background.

III. EXPERIMENTAL RESULTS

The RMSA scans are based upon the reflected particle angular distributions for a large range of incident angles. It is therefore appropriate to begin this section by presenting a typical HD angular distribution for one (arbitrarily chosen) incident angle. This should help clarify the kinematics which are an integral part of the RMSA data. Such an angular distribution is shown in Figure 1.

The discrete peaks seen in this figure are due to elastic and rotationally inelastic diffraction from the relatively flat and well-ordered Ag(111) surface. Similar scattering patterns have been previously reported for hydrogen isotopes reflecting from MgO(001)[24], LiF(001)[25], and Pt (111)[16,26,27] The initial ensemble of HD molecules is predominantly in the $|J,m\rangle = |0,0\rangle$ state. The low population of higher rotational states is due to both the high quality of our supersonic jet expansion, and to the absence of the $\Delta J=2$ selection rule for HD. Rotationally inelastic peaks are labelled $J_i \rightarrow J_f$, where these labels represent the initial and final rotational states of the reflected particles. These inelastic transitions are associated with the (00),(10) and $(\bar{1}0)$ diffraction peaks. Their final scattering angles are given by the momentum and energy conservation constraints which govern the scattering kinematics. These are (i) conservation of parallel momentum

$$\hbar K_i = \hbar K_f + \hbar G \qquad (1)$$

and (ii) conservation of total energy

$$k_i^2 = k_f^2 + (2M/\hbar^2)\,[E(J_f) - E(J_i)] \qquad (2)$$

where $\underset{\sim}{k}_i$ and $\underset{\sim}{k}_f$ are the initial and final wave vectors, M is the mass of HD, $E(J_f) - E(J_i)$ is the change in rotational energy, $\underset{\sim}{K}_i$ and $\underset{\sim}{K}_f$ are the components of $\underset{\sim}{k}_i$ and $\underset{\sim}{k}_f$ parallel to the surface, and $\underset{\sim}{G}$ is a reciprocal lattice vector. The above equations do not include phonon interactions which are weak processes for the collision energies and surface temperatures used in this study. The peak assignments shown in Figure 1 have been independently verified with time-of-flight velocity measurements.

The lower portion of Figure 1 is an Ewald representation of the scattering kinematics. This provides us with a very useful visualization of the scattering processes which are occurring. The radii of the five semicircles represent the magnitudes of the final k-vectors associated with the different transitions. Energy conservation requires that the final elastic and rotationally inelastic peaks fall on the appropriate semicircular arc, as given by Eq. (2). In addition, parallel momentum conservation, Eq. (1), requires that each peak fall on either the specular or $\underset{\sim}{G} \neq 0$ diffraction rods (Brillouin zone boundaries). The intersection of the semicircles and vertical rods, therefore, provide a graphical determination of the allowed final scattering angles. The indicated angles are those appropriate for a monoenergetic HD beam having $|k_i| = 12.7$ Å^{-1} and are in excellent agreement with the experimental results, justifying neglect of phonon interactions in the above discussion. The angular width and exact shape for each diffraction peak can be determined by carrying out a full convolution of the true data with the incident beam's velocity distribution and other instrumental resolution parameters. The reflected peaks have angular profiles which are not significantly broadened by surface domain size effects, indicating that the Ag(111) surface is well ordered. Scattering experiments have also been carried out along the $\langle 11\bar{2} \rangle$

and <10$\bar{1}$> directions: no apparent change is seen in the inelastic transition probabilities associated with the specular channel.

Two striking results are evident from the angular distribution shown in Figure 1. These are the extremely high rotationally inelastic cross-sections for HD relative to H_2 and D_2, and the presence of only weak diffraction for $\underset{\sim}{G} \neq 0$. The first observation can be attributed to the offset of the HD center-of-mass from its geometric center. The second observation indicates that the HD/Ag(111) potential has low corrugation. This will allow us to treat Ag(111) to first approximation as a flat surface in the scattering calculations presented later.

In Figure 2, RMSA scans (again, rotationally mediated selective adsorption) are shown for HD incident along the <10$\bar{1}$> and <11$\bar{2}$> azimuthal directions. Each of these scans consist of three independent data collection runs in which the intensities (peak heights) of the J=0→0, 0→1, and 0→2 transitions have been plotted verses E_{z_i}, the perpendicular component of the incident beam energy. The actual data were collected by varying θ_i, the incident polar angle, in ca. 0.2^o increments in the manner described earlier under experimental procedures.

The sharp undulations seen in Figure 2 are due to the phenomena of RMSA[16,17,18]. To a first approximation, these bound state scattering resonances arise when $\hbar^2 k^2_{z_f}/2M$, as calculated from Eqs. (1) and (2) for a given translation-rotation energy exchange process, is negative and precisely matches a bound energy level of the HD/Ag(111) physisorption potential. Resonance dips are observed in a J=0→n transition when the J=0→n+1 transition "deposits" the molecule into a bound level of the gas-surface potential

(i.e., J=0→n + 1 leads to a *closed* rotational scattering channel). (Hereafter, we shall use J_b to denote J_f when J_f is the rotational label for a *bound molecule*). As seen in Figure 2, the J_b=n + 1 resonances most strongly perturb the J=0→n transitions, causing pronounced minima to appear. Smaller complementary peaks can also be observed in J=0→n - 1 transitions. It therefore appears that the J_b=n + 1 resonance states decay primarily to states other than the nearest open channel, J=0→n.

Figures 2 and 3 have intentionally been plotted with E_{z_i} rather than θ_i along the horizontal axis in order to demonstrate that the resonance positions are independent of both azimuthal crystal orientation and incident momentum parallel to the crystal surface. This requirement of the proposed RMSA process is clearly met, since in Figure 2 the dip positions are invariant with respect to azimuthal orientation, and in Figure 3 the dip positions are shown to be invariant for three different incident beam energies (dip positions are unchanged even though equivalent E_{z_i} values occur at different θ_i settings). In Figure 3 it can also be seen that the effect of increasing the total collision energy with E_{z_i} held constant (i.e., increasing the parallel component of incident momentum) is to increase the likelihood of rotational excitation relative to elastic scattering.

In Table 1 we present our main experimental results, which are the resonance energies for J_b=1,2 and 3 as determined from the positions of minima in the J=0→0, 0→1, and 0→2 RMSA scans, respectively. These resonance energies were arrived at by averaging the data taken with different beam energies along both the <11$\bar{2}$> and <10$\bar{1}$> directions. Appearing next to these values are the approximate bound vibrational levels of the HD/Ag(111) physisorption potential as a function bound rotor state. These

energy levels were calculated by subtracting free rotor HD energies[28] from the appropriate resonance energies.

The discrepancies between the results for different J_b states imply that HD behaves as a slighly hindered rotor in the bound levels. It is apparent that there is a small but consistent shift in the energy of a given bound level as a function of J_b, a shift which is well outside the experimental uncertainty of our resonance energies. The small size of these shifts indicates that the hindering is relatively weak. This is independently confirmed by recent low energy electron loss experiments involving hydrogen physisorbed on Ag(111)[29] and Cu(001)[30].

The origin of these shifts and the way in which we can use them to extract the anisotropic part of the laterally averaged HD/Ag(111) potential will be described in the following section.

IV. THEORETICAL BACKGROUND

If inelastic processes between the surface and incident molecules are neglected, it is straightforward to write down the coupled equations for scattering of a diatomic molecule from a corrugated surface.

Assuming periodic corrugation and treating the molecule as a rigid rotor, the Hamiltonian for motion of the molecule is

$$H = \frac{-\hbar^2}{2M}\nabla^2 - \frac{\hbar^2}{2I}\frac{1}{\sin\theta}\frac{\partial}{\partial\theta}\sin\theta\frac{\partial}{\partial\theta} + \sum_{\underset{\sim}{G}} V_{\underset{\sim}{G}}(z,\theta,\phi)e^{i\underset{\sim}{G}\cdot\underset{\sim}{R}} \qquad (3)$$

Here z is the normal distance from the surface to the molecule center of mass, $\underset{\sim}{R} = (x,y)$ is a surface lattice vector, and $\underset{\sim}{G}$ a reciprocal lattice vector. θ and ϕ are the polar and azimuthal angles of the molecular axis relative to the z axis. The molecular wave function may then be expanded in products of spherical harmonics and plane waves of the two dimensional surface net:

$$\Psi(z,\theta,\phi,\underset{\sim}{R}) = \sum_{\underset{\sim}{G}Jm} \chi_{\underset{\sim}{G}Jm}(z)\, Y_J^m(\theta,\phi)\, e^{i(\underset{\sim}{G}+\underset{\sim}{K})\cdot\underset{\sim}{R}} \tag{4}$$

where $\underset{\sim}{K}$ is the incident parallel component of the wave vector. This leads to a set of coupled equations

$$\left[\frac{d^2}{dz^2} + k^2_{\underset{\sim}{G}J}\right]\chi_{\underset{\sim}{G}Jm}(z) = \sum_{\underset{\sim}{G}'J'm'} \frac{2M}{\hbar^2}\langle Jm|V_{\underset{\sim}{G}-\underset{\sim}{G}'}(z,\theta,\phi)|J'm'\rangle\chi_{\underset{\sim}{G}'J'm'}(z) \tag{5}$$

where $$k^2_{\underset{\sim}{G}J} = \frac{2ME}{\hbar^2} - (\underset{\sim}{K}+\underset{\sim}{G})^2 - J(J+1)\frac{M}{I} \tag{6}$$

Since diffraction is very much weaker than rotational excitation for the asymmetric rotor-metal system, it is valid to neglect coupling terms for which $\underset{\sim}{G} - \underset{\sim}{G}' \neq 0$ in studying the rotationally inelastic spectra. This assumption of a flat surface is a significant simplifying feature, since the number of open channels for HD at beam energies of 100 meV is reduced from about 100 to 4. The potential $V_0(z,\theta,\phi)$ is then assumed to be independent of ϕ, ensuring conservation of the azimuthal quantum number m.

The potential to be used for interpreting the rotationally inelastic spectra is then $V_0(z,\theta)$. For a symmetric rotor, an expansion of this in Legendre polynomials of $\cos\theta$ reduces to a sum over even terms only.

$$V_0(z',\theta) = \sum_{l=0,2,4\ldots} V_l(z')\, P_l(\cos\theta) \tag{7}$$

Here z' is the normal distance from the surface to the center of mass, which is the geometric center of the molecule in this case.

In the previous quantum calculations of scattering of diatomic molecules from solid surfaces, the expansion is truncated after the second term, by analogy with atom-molecule potential surfaces[17,19,31]. This is exact for asymptotically large z, where the molecule-surface interaction is dominated by the attractive polarization force [32]. At small z, however, the repulsive potential arising from overlap of electronic densities of the molecule and of the surface is dominant. It has not yet been established whether higher terms are present here or whether, if present, it is warranted to neglect them. However, since we aim to provide the simplest possible parameterization of the potential $V_0(z,\theta)$ which adequately represents the rotationally inelastic selective adsorption features, we regard it sufficient at this stage to retain only $\ell=0,2$ in Eq. (7). We further follow the form of previous calculations[31] by making $v'_2(z) = \beta v_0(z)$, where $v_0(z)$ is the laterally averaged potential for interaction of a structureless particle with the surface. The potential is then entirely determined by β and $v_0(z)$.

The corresponding potential for a chemically equivalent (isotopic) asymmetric rotor is obtained by transforming $V_0(z',\theta)$ from the geometric center of the diatom to the displaced center of mass;

$$V_0(z',\theta) = V_0(z')[1+\beta P_2(\cos\theta)] \tag{8a}$$

$$= V_0(z) + \sum_{\ell=0,1,2\ldots} V'_\ell(z) P_\ell(\cos\theta) \tag{8b}$$

Here z' is the normal distance from the surface to the geometric center of HD, and z is the normal distance from the surface to the center of mass:

$$z' = z + \delta \cos\theta \tag{9}$$

where δ is the displacement of the center of mass from the geometric center. For HD, $\delta = 0.233 a_0$.

The laterally averaged potential $v_0(z)$ is separated out to obtain a decoupled zeroth-order Hamiltonian,

$$H^0 = \frac{-\hbar^2}{2M}\frac{d^2}{dz^2} - \frac{\hbar^2}{2I}\frac{1}{\sin\theta}\frac{\partial}{\partial\theta}\sin\theta\frac{\partial}{\partial\theta} + v_0(z) \tag{10}$$

The full Hamiltonian is

$$H = H^0 + V \tag{11}$$

with

$$V = \sum_{l=0}^{\infty} v_l'(z) P_l(\cos\theta) \tag{12}$$

Eigenfunctions of H^0 will be referred to as a bound-vibration-rigid rotor states (BVRR states), following ref. (17). They are direct products of eigenfunctions of $v_0(z)$, which are exactly analogous to the bound states probed in atomic diffractive selective adsorption, and rigid rotor functions.

If the resonant states were unhindered rigid rotors in bound states of $v_0(z)$, the resonance energies would be equal to the BVRR energies. However, the BVRR states are not eigenvalues of the full Hamiltonian: the coupling V, Eq. (11), will shift the resonance energies from the BVRR energies. The extent of the shift is an indication of the amount of interaction between rotational and vibrational motions in the quasibound state. It was recently shown[17] that for a potential of the form in Eq. (8) appropriate to HD on metals, resonances in the inelastic transition probabilities occur at energies very close to the first order perturbed BVRR energies.

$$E_\nu^c \sim E'_{nJ} = \epsilon_n + \frac{\hbar^2}{2I}J(J+1) + \left\langle nJ\left|\sum_{l=0}^{\infty} v_l'(z) P_l(\cos\theta)\right|nJ\right\rangle \tag{13}$$

Here E_ν^c is the calculated resonance energy, $E'_{n\,J}$ is the BVRR energy plus the first order correction from the potential V, Eq. (12), ϵ_n is an eigenvalue

of $v_0(z)$ and $|nJ\rangle$ is a BVRR eigenfunction, with n denoting the vibrational state, and J the rotor state.

We used the same method of solving the close coupled equations here as in ref. (17), namely the single R-matrix, generating BVRR states, energies $E^0_{n\,J}$ and $E'_{n\,J}$, and rotationally inelastic transition probabilities. We did this for two different forms of potential $v_0(z)$, with a range of values of β in each case. The R-matrix calculation employs a basis of the direct product of free rotor states with a translational basis in which the bound vibrational states are expanded on a finite inner region. Sine functions were used for the translational basis. Increasing the size of this region and the size of the translational basis allows the bound vibrational states to be calculated to any specified accuracy. This product basis is then used to construct the R-matrix, or Green's function, at the outer boundary of the region, R. Matching to the asymptotic form of the wave function then gives the S-matrix and probabilities for rotational transitions. Full details of the R-matrix calculations will appear later[33].

The laterally averaged potential $v_0(z)$ was modelled by a Morse potential and also by a variable exponent potential. The Morse potential,

$$V_0(z) = D\left[e^{-2\alpha(z-z_e)} - 2e^{-\alpha(z-z_e)}\right] \tag{14}$$

a two parameter potential (z_e does not affect the eigenvalues) used in the previous calculation for HD on Pt(111), was used here primarily for its simplicity. The variable exponent potential,

$$V_0(z) = D\left\{\left[1+\frac{\lambda}{p}(z-z_e)\right]^{-2p} - 2\left[1+\frac{\lambda}{p}(z-z_e)\right]^{-p}\right\} \tag{15}$$

a three parameter potential including Eq. (14) as a special case, ($p \to \infty$), is a flexible form which has been used with considerable success to fit bound states from atomic[34] and molecular[35] diffractive selective adsorption. An analytic approximation to its eigenvalues has been given[36].

V. THEORETICAL RESULTS AND COMPARISON WITH EXPERIMENT

Calculations were carried out with three sets of potential parameters, which are summarized in Table 2. The position of the potential minimum, z_e, was chosen such that the finite value of the potential at z=0 is at least three times as large as the maximum normal incident beam energy E_{z_i}. The three sets of potential parameters were determined by fitting our diffractive selective adsorption data for (predominantly J_b=0) D_2 on Ag(111)[20]. Potential A is of the variable exponent form, Eq. (15). The values of its three parameters were arrived at by carrying out a non-linear least squares fit of the experimentally determined D_2/Ag(111) eigenvalues to the approximate analytical eigenvalues. The parameters for potential B (also of variable exponent form) and Morse potential C were determined in a similar manner, but with their well depths held constant at the value given by our Debye-Waller attenuation measurements, D=46 meV[20]. Figure 4 shows the three potentials A, B and C as a function of z. Figure 5 shows the coupling terms $v'_\ell(z)$ as a function of z for potential A with β= -0.05.

Results of a typical scattering calculation are shown in Figure 6. This shows the transition probabilities $J=0 \to J_f$, J_f=0,1,2,3 as a function of the perpendicular component of incident energy, E_{z_i}, for potential A with β= -0.05. The deep minima just above threshold in each channel correspond to the J+1 resonances seen in the experimental data. The theoretical results also show weaker maxima and minima at higher energies, corresponding to J+2 and J+3

resonances. When a phenomenological dissipative term is included in the Hamiltonian, Eq. (11), the weaker features disappear and only the J+1 minima remain[33]. In the absence of any dissipative terms in Eq. (11) the R-matrix calculation preserves unitarity, so that at energies below 11 meV, when only the J=0 channel is open, the transition probability is necessarily unity.

For each potential A, B, and C, a series of R-matrix calculations were carried out at several values of β. Minimization of the χ^2 function

$$\chi^2 = \sum_\nu \left[\frac{E_\nu - E_\nu^c}{\Delta_\nu} \right]^2 \qquad (16)$$

where E_ν are the experimental resonance energies, Δ_ν their standard deviation and E^c_ν the calculated resonance energies, was used as a measure of the goodness of fit of a given set of parameters. Summation was performed over the 0→1 and 0→2 resonances only, since the calculation does not provide E^c_ν for the 0→0 transition (see above). Table 3 shows the variation of χ^2 with β. A minimum value is attained for β between -0.05 and -0.10. It is apparent that all three potentials achieve a comparable fit of the experimental resonance data. Slightly different values of an optimum β are obtained, with the size of the estimated value increasing with well depth. For potential A, the best fit is obtained with β= -0.05, for potential B, β lies between -0.05 and -0.10, and for potential C, β= -0.10. A comparison of E_ν and E^c_ν for potential A with β= -0.05 is given in Table 4.

These calculations were all carried out using an R-matrix direct product basis of 60 translational (sine) functions x 6 rotational functions. The R-matrix boundary, R, was taken at $9.00a_0$. Reference to Figure 4 shows that the size of the residual potential at the boundary R is considerably greater for the variable exponent potentials A and B than for the Morse potential C. This has a relatively large effect on the highest vibrational eigenvalues as shown in Table 5 and also, indirectly, a slight effect on the resonance energies E^c_ν, since the residual potential should be negligible at the asymptotic matching surface. Calculations for potentials A and B, with the R-matrix boundary chosen in each case such that $v_0(R)$ is equal to the residual Morse potential for $R=9.00a_0$ (-1.7 meV), were then performed for the best value of β from Table 3, $\beta= -0.05$. These results are shown in Table 6. A marked improvement in accuracy is seen, making both potentials A and B, with $\beta= -0.05$, of comparable accuracy to the Morse potential C with its best value of $\beta= -0.10$. The values of E^c_ν and E'_ν for potential A with $\beta= -0.05$ and $R=12.0a_0$ are listed in Table 4 next to those previously mentioned for $R=9.0a_0$.

VI. DISCUSSION

Comparison of our experimental and theoretical resonance energies reveals that β, the asymmetry parameter, has a value which falls in the range $-0.10 \leqslant \beta \leqslant -0.05$. This conclusion is independent of the isotropic potential (A, B, or C) which is used in the scattering calculation. Further comparison of these results also reveals that calculations employing either of the variable exponent potentials A or B, or Morse potential C, give the same quality fit to our experimental resonance energies. This relative insensitivity of the calculated resonance

energies to slight changes in the isotropic potential, $v_0(z)$, as compared with their sensitivity to the asymmetry parameter, suggests that the magnitude and sign of β can be well determined from a combination of RMSA and DSA measurements.

The important and complementary difference between RMSA and DSA measurements is that the former process places molecules of $J_b>0$ (or more specifically, $J_b>J_i$) into bound levels of the physisorption potential, while the latter process conserves the incident J-state ($J_b=J_i$). DSA measurements can therefore be used to obtain the isotropic part of the potential when $J_i=0$, due to the absence of J- and m- dependent shifts in this case. One can then build upon the resulting $v_0(z)$ potential by making RMSA measurements, which are sensitive to the anisotropy of the potential. This sensitivity manifests itself as J_b-dependent shifts (for $J_i=0$ there is no m- dependence) in the observed resonance energies. Such a procedure has been followed in this paper. We are currently refining the $v_0(z)$ potential utilizing additional DSA measurements for H_2 and D_2 on Ag(111), and will publish our final results elsewhere[20].

Both the sign and magnitude of the asymmetry parameter β are of interest. The negative value of β found in these studies indicates that the averaged interaction potential is slightly deeper for hydrogen oriented parallel to the surface than perpendicular to it. Thus hydrogen has a slight propensity to reside with its internuclear axis parallel to the surface in the bound states of $v_0(z)$. In a sense this is a surprising result. At large molecule-surface distances van der Waals attractive forces dominate the interaction. These forces tend to orient the molecular axis perpendicular to the surface since the polarizability of hydrogen along its internuclear axis, $\alpha_{\parallel}$, is larger than the polarizability perpendicular to it, $\alpha_{\perp}$. In contrast to this, at

small molecule-surface distances electron repulsion dominates the interaction, tending to orient the molecular axis parallel to the surface. The two forces, van der Waals attraction and electron repulsion, therefore, favor different orientations of physisorbed hydrogen. This qualitative reasoning is supported by Gordon-Kim calculations for hydrogen adsorbed in parallel and perpendicular orientations on a jellium surface[37]. The negative value of β observed in our experiments indicates (at least in an averaged sense with respect to bound level, n) that the orientational anisotropy of hydrogen in the bound states sampled here is more sensitive to the repulsive part of the potential.

This conclusion is contrary to the assumption made in most previous calculations using potentials having the form of Eq. (8a), namely that the anisotropy parameter β is determined essentially by the asymptotic van der Waals interaction[31,32]. However, it is important to note that a potential of the form (8a) with β treated as a constant does not possess the flexibility to give the correct lowest energy orientation at both large and small distances from the surface. It is clear that the value of β obtained here is really a distance averaged quantity, an average in which the compensating contributions from large and small distances are slightly dominated by the latter. With regard to this, it would be of value to perform an electron energy loss experiment involving a low coverage of physisorbed hydrogen on Ag(111) which would accurately determine the m-splittings for the n=0 level, from which a level specific value of β could be derived. It is our opinion that treating β as a constant will ultimately prove to be inadequate, and it must necessarily be treated as a distance dependent quantity in a more accurate description of the hydrogen/Ag(111) interaction.

The actual magnitude of the anisotropy parameter, β, quantifies the orientation dependence of the hydrogen/Ag(111) interaction. As mentioned

previously, at asymptotically large distances from the surface this term comes from the asymmetry of the hydrogen molecular polarizability tensor. In the first quantum scattering calculations of Wolken[31] it was assumed that β was given by the ratio of the static parallel and perpendicular hydrogen polarizabilities[38], which yields $\beta=+0.24$. This value has been used in many subsequent quantum scattering calculations. It is apprently not correct. This has been recently discussed in detail by Harris and Feibelman[32], who took into account both the asymmetry of the molecular polarizability and the angle dependence of the surface response to a dipole field, finding $\beta=+0.05$. The results of our study indicate the need for a still more comprehensive theoretical treatment in which repulsive interactions are also taken into account. We must note, however, that the averaged anisotropic contributions in this system are quite small as evidenced both by the small magnitude of β and by the relatively free rotation of the vibrationally bound HD.

VII. CONCLUSION

In this paper rotationally mediated selective adsorption scattering resonances have been used to determine the vibrational levels of the HD/Ag(111) physisorption potential as a function of bound rotational state. These experimental energy levels have been used in conjuction with exact quantum scattering calculations to study the anisotropic part of the laterally averaged molecule-surface potential. A value for the asymmetry parameter has been determined which is in close agreement with recent theoretical predictions. Its value falls in the range $-0.10 \leq \beta \leq -0.05$.

The success of this study suggests that a general procedure for examining the interaction of molecular hydrogen with a variety of substrate materials has been developed. Diffractive selective adsorption studies of J=0

H_2 or D_2 should first be conducted in order to determine the laterally averaged isotropic part of the potential. Next, rotationally mediated selective adsorption measurements should be carried out for different bound rotational states. Finally, close-coupled scattering calculations can be used to analyze the J_b-dependent shifts in the RMSA data in order to extract the orientation dependence of the molecule-surface interaction potential.

In the near future we hope to refine our analysis of the hydrogen/Ag(111) potential by comparing deconvoluted rotationally inelastic transition probabilities with those calculated using our R-matrix techniques. Additional diffractive selective adsorption studies are also planned to further refine the isotropic part of the potential which was used in this paper.

ACKNOWLEDGEMENTS

The authors wish to thank Kevin Gibson and Yaw-Wen Yang for their assistance during the course of these experiments. This work was supported, in part, by the Office of Naval Research under grant ONR-N00014-77-C-0240, by the Materials Research Laboratory Program of the National Science Foundation at the University of Chicago under grant DMR-7924007, and by a Camille and Henry Dreyfus Young Facility Grant to S.J. Sibener.

REFERENCES

[1] M.J. Cardillo, Ann. Rev. Phys. Chem. 32, 331 (1981).

[2] H. Hoinkes, Rev. Mod. Phys. 52, 933 (1980).

[3] N. Esbjerg and J.K. Nørskov, Phys. Rev. Lett. 45, 807 (1980).

[4] R.B. Laughlin, Phys. Rev. B25, 2222 (1982).

[5] D.R. Hamann, Phys. Rev. Lett. 46, 1227 (1981).

[6] T.H. Ellis, S. Iannotta, G. Scoles, and U. Valbusa, Phys. Rev. B24, 2307 (1981).

[7] T.H. Ellis, G. Scoles, and U. Valbusa, Surf. Sci. 118, L251 (1982).

[8] K. Gibson and S.J. Sibener; to be published.

[9] I. Estermann and I.O. Stern, Z. Phys. 61, 95 (1930).

[10] J.E. Lennard-Jones and A.F. Devonshire, Nature (London) 137, 1069 (1936); Proc. Roy. Soc. (London) A158, 253 (1937).

[11] C. Schwartz, M.W. Cole, and J. Pliva, Surf. Sci. 75, 1 (1978).

[12] R. Rydberg, Z. Phys. 73, 376 (1931).

[13] O. Klein, Z. Phys. 76, 226 (1932).

[14] A.L.G. Rees, Proc. Soc. (London) 59, 998 (1947).

[15] H. Chow and E.D. Thompson, Surf. Sci. 59, 225 (1976).

[16] J.P. Cowin, C.F. Yu, S.J. Sibener, and J.E. Hurst, J. Chem. Phys. 75, 1033 (1981).

[17] K.B. Whaley, J.C. Light, J.P. Cowin, and S.J. Sibener, Chem. Phys. Lett. 89, 89 (1982).

[18] R. Schinke, Chem. Phys. Lett. 87, 438 (1982).

[19] R.B. Gerber, A.T. Yimon, Y. Shimoni, and D.J. Kouri, J. Chem. Phys. 73, 4397 (1980).

[20] C.F. Yu, C.S. Hogg, K.B. Whaley, and S.J. Sibener; to be published.

[21] C.A. Becker, Ph.D. Thesis, University of Chicago, 1980; D. Auerbach, C. Becker, J. Cowin, and L. Wharton, Appl. Phys. 14, 141 (1977).

[22] Beam Dynamics, Inc., Minneapolis, Minnesota, U.S.A.

[23] E.R. Jones, J.T. McKinney, and M.B. Webb, Phys. Rev. 151, 476 (1966).

[24] R.G. Rowe and G. Ehrlich, J. Chem. Phys. 62, 735 (1975); J. Chem. Phys. 63, 4648 (1975).

[25] G. Boato, P. Cantini and L. Mattera, J. Chem. Phys. 65, 544 (1976).

[26] J.P. Cowin, C.F. Yu, J.E. Hurst and S.J. Sibener, Proc. VIII Intl. Symp. on Molecular Beams, 1981, Cannes, pp. 136-8.

[27] J.P. Cowin, C.F. Yu, S.J. Sibener and L. Wharton; to be published.

[28] H.W. Woolley, R.B. Scott and F.G. Brickwedde, J. Res. Natl. Bur. Stand. (U.S.) 41, 379 (1948).

[29] Ph. Avouris, D. Schmeisser and J.E. Demuth, Phys. Rev. Lett. 48, 199 (1982).

[30] S. Andersson and J. Harris, Phys. Rev. Lett. 48, 545 (1982).

[31] G. Wolken, Chem. Phys. Lett. 21, 373 (1973); J. Chem. Phys. 59, 1159 (1973); 62, 2730 (1974).

[32] J. Harris and P.J. Feibelman, Surf. Sci. 115, L133 (1982).

[33] K.B. Whaley and J.C. Light; to be published.

[34] E. Ghio, L. Mattera, C. Salvo, F. Tommasini and U. Valbusa, J. Chem. Phys. 73, 556 (1980).

[35] L. Mattera, F. Rosatelli, C. Salvo, F. Tommasini, U. Valbusa and G. Vidali, Surf. Sci. 93, 515 (1980).

[36] L. Mattera, C. Salvo, S. Terreni and F. Tommasini, Surf. Sci. 97, 158 (1980).

[37] D. Kumamoto, J.E. Van Himbergen, and R. Silbey, Chem. Phys. Lett. 68, 189 (1979).

[38] W. Kolos and L. Wolniewicz, J. Chem. Phys. 46, 1426 (1967).

TABLE 1

Experimental Resonance Energies and Bound Levels for $HD(J_b)/Ag(111)$ (meV)

	J_b=1			J_b=2			J_b=3		
	Ez	Eν	$p^{(a)}\sigma^{(b)}$	Ez	Eν	$p^{(a)}\sigma^{(b)}$	Ez	Eν	$p^{(a)}\sigma^{(b)}$
n = 7	10.17	-0.89	5 .15						
6	8.72	-2.34	6 .11						
5	6.21	-4.85	6 .13	29.67	-3.45	7 .23	64.16	-1.85	6 .33
4	2.48	-8.58	6 .07	25.95	-7.17	7 .24	60.04	-5.97	6 .24
3				20.87	-12.25	7 .25	55.19	-10.82	6 .26
2				14.37	-18.75	7 .28	48.56	-17.45	6 .27
1							40.21	-25.80	6 .30
0									

(a) p: number of data points used for averaging

(b) σ: Standard deviation.

TABLE 2

Parameters for the three potentials used to model the laterally averaged potential, $v_0(z)$.

Potential	Form	Parameters			
		D(meV)	$\lambda(a_0^{-1})$	p	$\alpha(a_0^{-1})$
A	Variable Exponent	43.045	0.6180	4.9950	-
B	Variable Exponent	46.000	0.7005	3.5312	-
C	Morse	46.000	-	-	0.5956

Equilibrium Distance $z_e = 2.3441a_0$.

Center of mass displacement for HD, $\delta = 0.233a_0$.

TABLE 3

Variation of the χ^2 function, Eq. (16), with the anisotropy parameter, β, for potentials A, B and C.

Potential	β	$\chi^2(meV^2)$
A	+0.35	842.9
A	+0.30	722.6
A	+0.20	427.4
A	+0.10	218.5
A	0.00	138.4
A	-0.025	125.1
A	-0.05	118.5
A	-0.075	118.0
A	-0.10	134.0
A	-0.20	229.7
A	-0.30	457.1
A	-0.35	594.1
B	+0.20	503.1
B	0.00	141.7
B	-0.025	121.2
B	-0.05	110.7
B	-0.075	109.4
B	-0.10	111.1
B	-0.20	215.8
C	+0.20	597.4
C	0.00	155.0
C	-0.025	142.3
C	-0.05	99.9
C	-0.075	91.5
C	-0.10	85.3
C	-0.15	102.2
C	-0.20	147.3
C	-0.30	337.0

TABLE 4

Positions of the experimentally observed and calculated resonance minima, and the corresponding BVRR energies for the J=0→1 and J=0→2 transition probabilities shown in Figure 6. Potential A was used with $\beta = -0.05$. R denotes the position of the R-matrix boundary, in a_0. The bound vibration state is labelled by n, the rotational state by J. Experimental resonances are denoted by E_ν, the calculated resonances by E^c_ν. E'_ν denotes the BVRR energy, Eq. (12). Values of E^c_ν and E'_ν are shown for calculations performed with $R=9.0a_0$, and $R=12.0a_0$ (See text).

Transition	ν	E_ν	E^c_ν R=9.0	E'_ν R=9.0	E^c_ν R=12.0	E'_ν R=12.0	n,J
	1	14.37	15.4	15.46	15.4	15.46	2,2
0→1	2	20.87	21.5	21.62	21.5	21.62	3,2
	3	25.95	26.0	26.08	26.0	26.14	4,2
	4	29.67	28.7	28.87	29.1	29.26	5,2
	5	40.21	40.3	40.24	40.3	40.24	1,3
	6	48.56	48.4	48.31	48.4	48.31	2,3
0→2	7	55.19	54.6	54.49	54.6	54.49	3,3
	8	60.04	59.0	58.95	59.0	59.01	4,3
	9	64.16	61.8	61.75	62.2	62.14	5,3

TABLE 5

Comparison of the vibrational eigenvalues of $v_0(z)$ calculated in a finite R-matrix translational basis with the analytic eigenvalues[a] for potentials A, B and C. Eigenvalues are shown for two values of R, the R-matrix boundary, for potentials A and B. The vibrational quantum number is n. The translational basis consists of 60 sine functions.

Potential	n	Analytic eigenvalues, ϵ_n	R-matrix eigenvalues	
			R = 9.00	R = 12.00
A	0	-36.9538	-36.949	-36.949
	1	-26.5775	-26.572	-26.572
	2	-18.3353	-18.346	-18.346
	3	-11.9879	-12.030	-12.030
	4	- 7.2943	- 7.422	- 7.376
	5	- 4.0109	- 4.517	- 4.135
	6	- 1.8918	- 1.212	- 2.194
	7	- 0.6878	+ 3.604	- 0.590
			R = 9.00	R = 12.79
B	0	-38.9176	-38.912	-38.912
	1	-27.2635	-27.261	-27.261
	2	-18.3965	-18.422	-18.422
	3	-11.8514	-11.926	-11.926
	4	- 7.1995	- 7.397	- 7.329
	5	- 4.0500	- 4.609	- 4.226
	6	- 2.0513	- 1.058	- 2.358
	7	- 0.8925	+ 4.003	- 1.162
			R = 9.00	
C	0	-39.8865	-39.867	
	1	-28.9667	-28.917	
	2	-19.7897	-19.721	
	3	-12.3556	-12.280	
	4	- 6.6644	- 6.599	
	5	- 2.7161	- 2.898	
	6	- 0.5106	- 0.191	
	7	- 0.0479	+ 4.118	

a) The analytic approximation[36] to the eigenvalues of the variable exponent potential is used here for potentials A and B.

TABLE 6

Values of χ^2, Eq. (16), shown for calculations performed with different R-matrix values, R, for potentials A and B.

Potential	β	R	$\chi^2(meV^2)$
A	-0.05	9.0	118.5
		12.0	90.2
B	-0.05	9.0	110.7
		12.79	91.5

FIGURE CAPTIONS

[1] Angular distribution of the reflected number density for HD scattering from Ag (111) along the $\langle 11\bar{2} \rangle$ direction. Rotationally inelastic transitions are labelled $J_i \rightarrow J_f$. Vertical lines denote the predicted peak locations for a monoenergetic beam with $k_i = 12.7$ Å^{-1}. The lower section is an Ewald representation of the displayed angular distribution.

[2] Rotationally elastic and inelastic transition intensities versus normal incident energy for HD incident along the $\langle 11\bar{2} \rangle$ and $\langle 10\bar{1} \rangle$ azimuthal directions. The vertical lines indicate the RMSA resonance energies, which are demonstrated here to be invariant with respect to incident azimuthal orientation.

[3] Rotationally elastic and inelastic transition intensities versus normal incident energy for three different beam energies: 40.6, 113.6 and 153.0 meV. The vertical lines indicate the RMSA resonance energies, which are demonstrated here to be invariant with respect to incident momentum parallel to the crystal surface.

[4] The isotropic component of the laterally averaged molecule-surface potential, $v_0(z)$, as a function of z, the normal distance to the metal surface. Potentials A and B are variable exponent potentials, Eq. (15), with well depths of 43.0 meV and 46.0 meV, respectively. Potential C is a Morse potential, Eq. (14), with well depth 46.0 meV. The full potential parameters are given in Table 2.

[5] The coefficients $v'_{\ell}(z)$ for the Legendre expansion of the potential, Eq.(8b), as a function of z, obtained from potential A with $\beta = -0.05$. The center of mass displacement from the HD geometric center is $\delta = 0.233a_0$.

[6] Transition probabilities for rotational excitation of HD incident on Ag (111), calculated for potential A, with $\beta = -0.05$. Transition probabilities were calculated at normal incident energy increments of 0.2 meV.

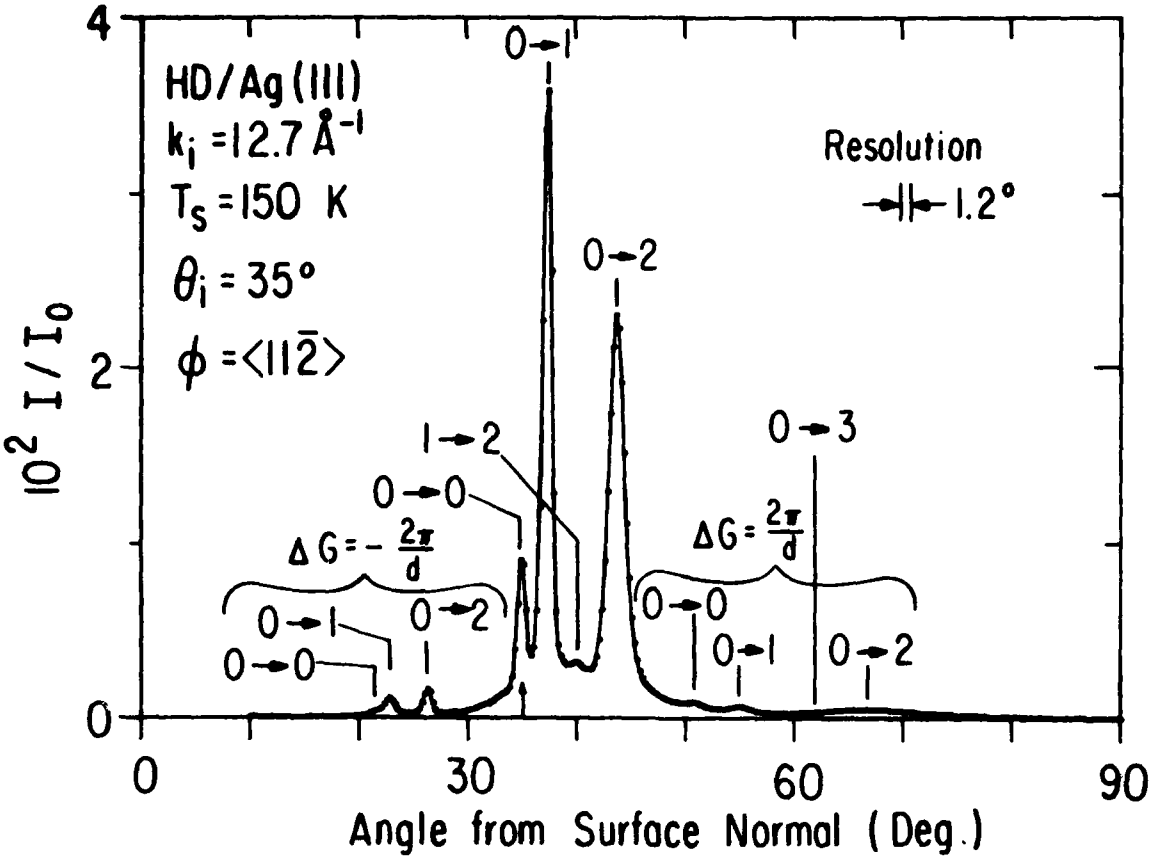
HD/Ag(111)
k_i = 12.7 Å^{-1}
T_s = 150 K
θ_i = 35°
ϕ = <11$\bar{2}$>
Resolution
1.2°
10^2 I/I$_0$
Angle from Surface Normal (Deg.)
0→1
0→2
0→3
1→2
0→0
$\Delta G = -\frac{2\pi}{d}$
$\Delta G = \frac{2\pi}{d}$

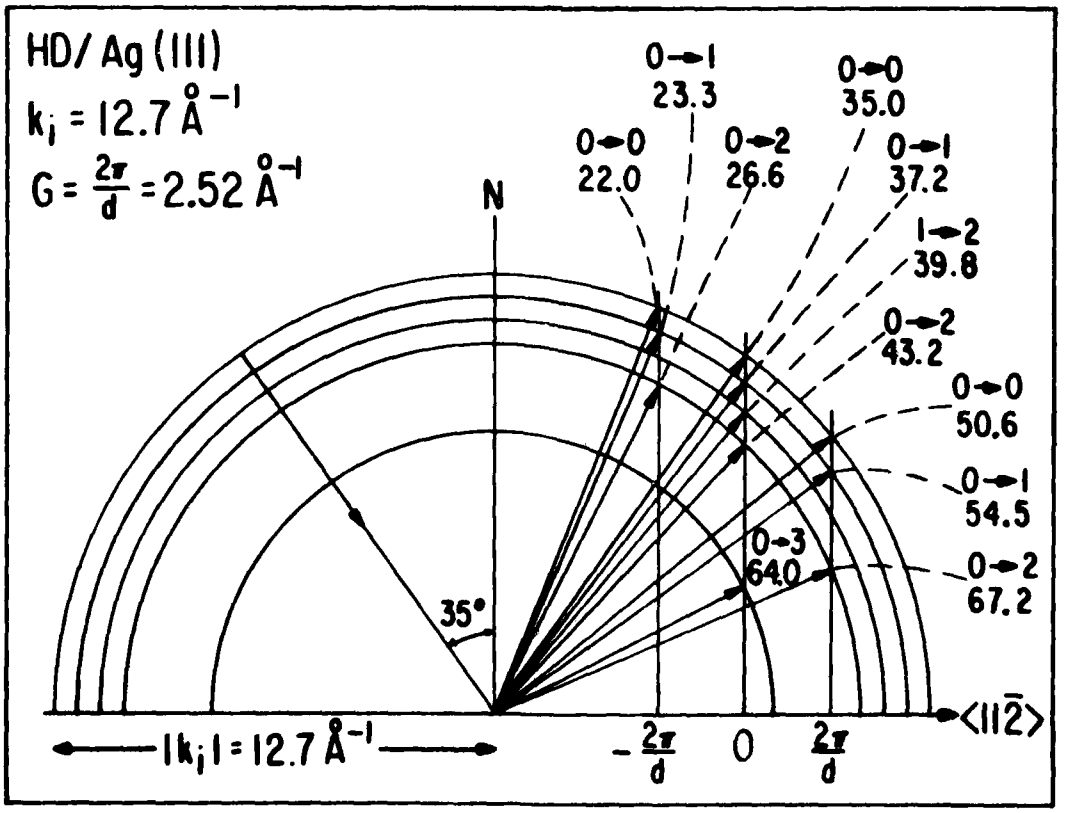
HD/Ag(111)
k_i = 12.7 Å^{-1}
$G = \frac{2\pi}{d}$ = 2.52 Å^{-1}
N
0→1 23.3
0→0 35.0
0→0 22.0
0→2 26.6
0→1 37.2
1→2 39.8
0→2 43.2
0→0 50.6
0→1 54.5
0→3 64.0
0→2 67.2
35°
<11$\bar{2}$>
$|k_i| = 12.7$ Å^{-1}
$-\frac{2\pi}{d}$
0
$\frac{2\pi}{d}$

Fig.1

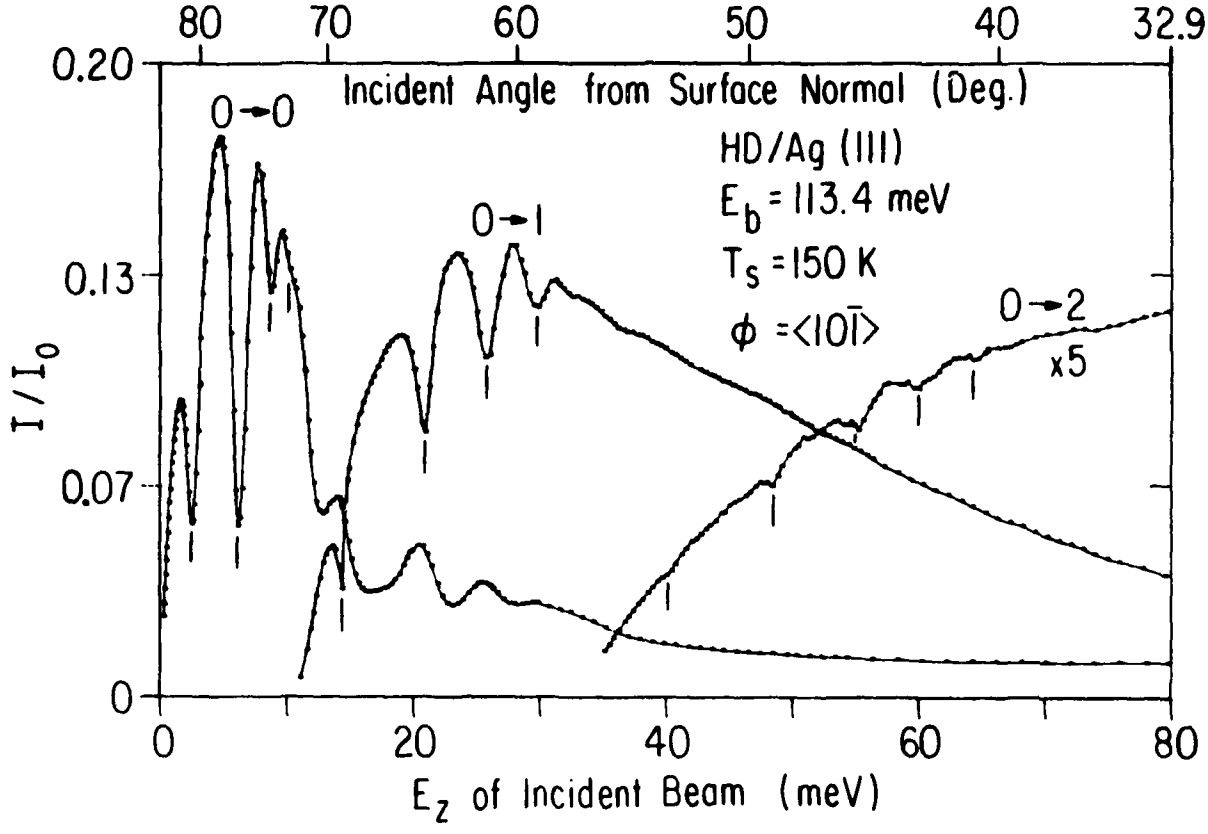
80
70
60
50
40
32.9
Incident Angle from Surface Normal (Deg.)
HD/Ag (111)
E_b = 113.4 meV
T_s = 150 K
ϕ = <10$\bar{1}$>
0→0
0→1
0→2
x5
I/I$_0$
0.20
0.13
0.07
0
0
20
40
60
80
E_z of Incident Beam (meV)

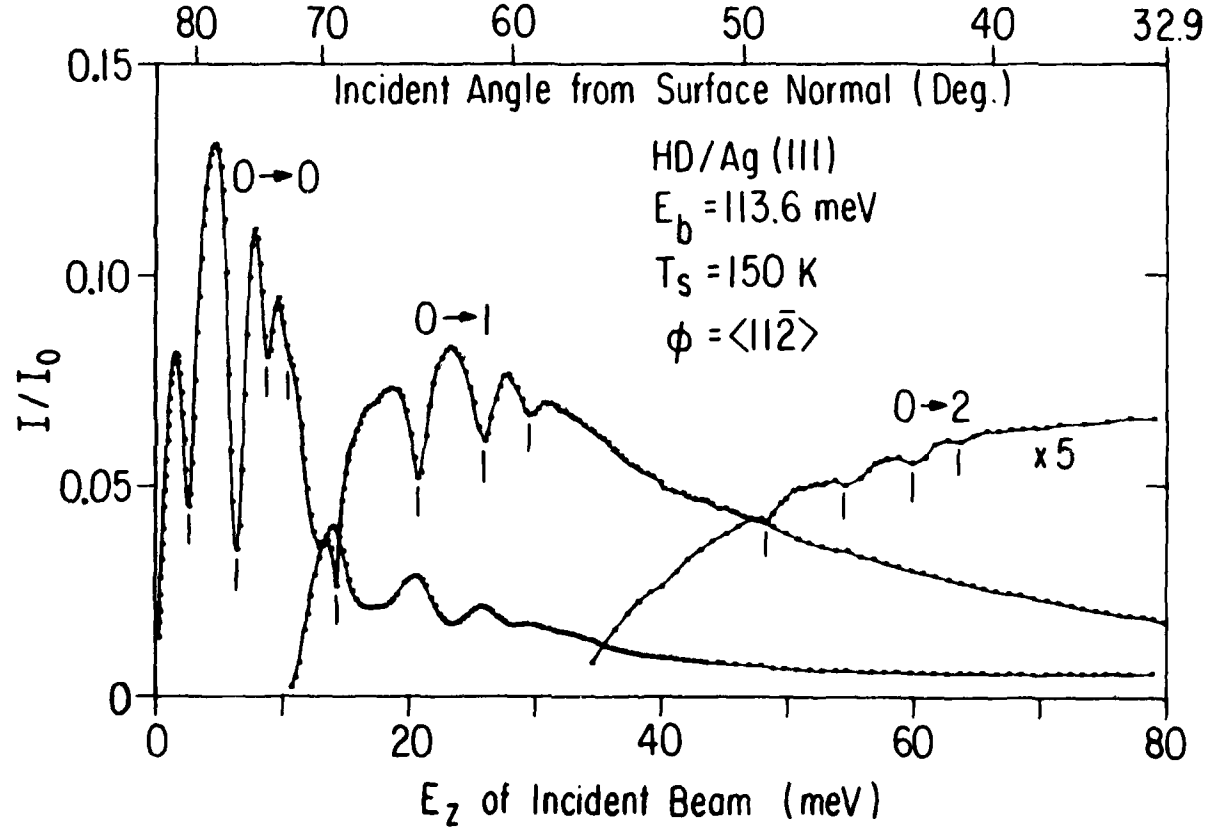
80
70
60
50
40
32.9
Incident Angle from Surface Normal (Deg.)
HD/Ag (111)
E_b = 113.6 meV
T_s = 150 K
ϕ = <11$\bar{2}$>
0→0
0→1
0→2
x5
I/I$_0$
0.15
0.10
0.05
0
0
20
40
60
80
E_z of Incident Beam (meV)

Fig.2

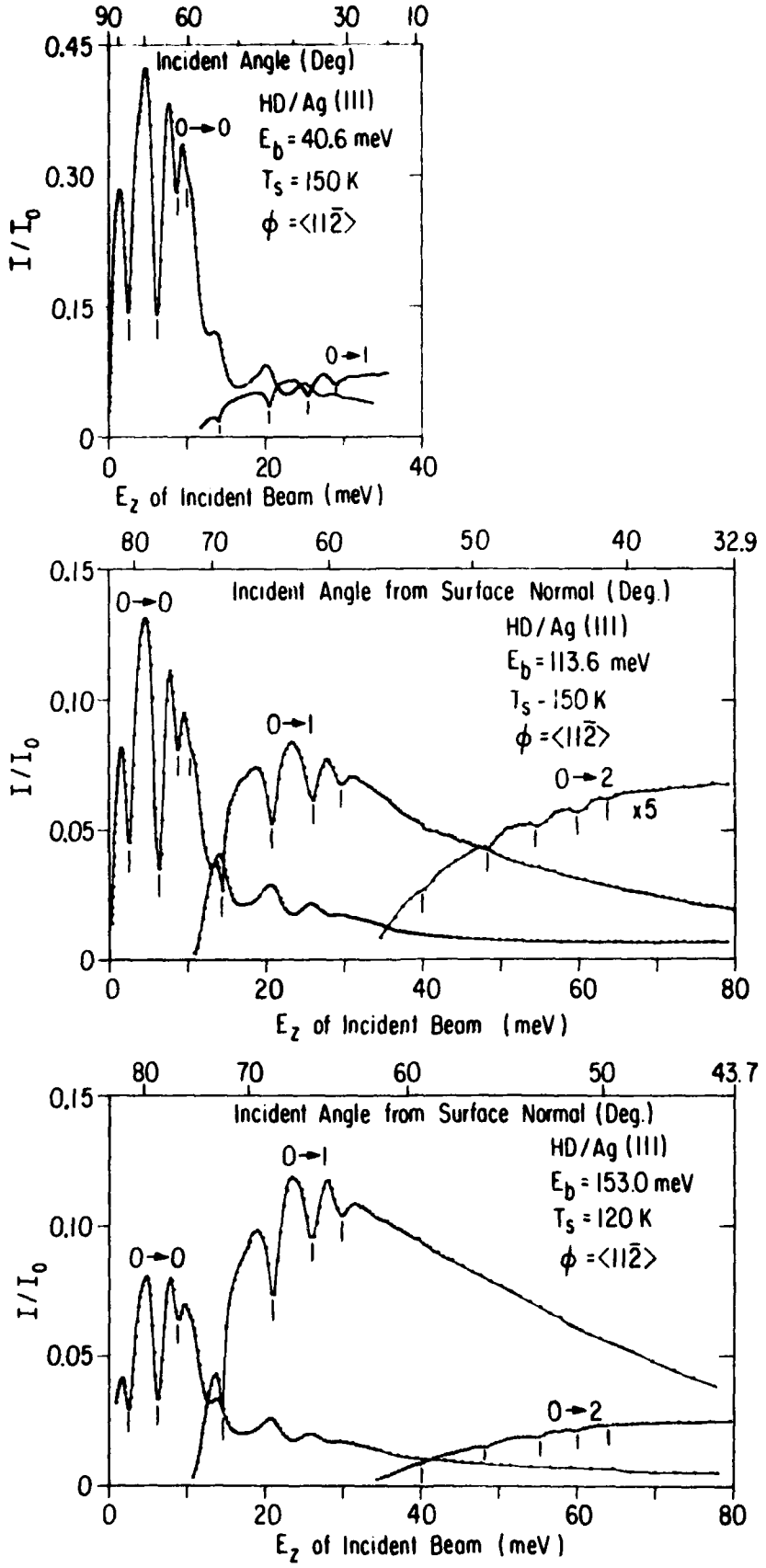
90
60
30
10
0.45
0.30
0.15
0
Incident Angle (Deg)
HD/Ag (111)
E_b = 40.6 meV
T_s = 150 K
ϕ = <11$\bar{2}$>
0→0
0→1
I/I_0
0
20
40
E_z of Incident Beam (meV)
80
70
60
50
40
32.9
0.15
0.10
0.05
0
Incident Angle from Surface Normal (Deg.)
HD/Ag (111)
E_b = 113.6 meV
T_s - 150 K
ϕ = <11$\bar{2}$>
0→0
0→1
0→2
x5
I/I_0
0
20
40
60
80
E_z of Incident Beam (meV)
80
70
60
50
43.7
0.15
0.10
0.05
0
Incident Angle from Surface Normal (Deg.)
HD/Ag (111)
E_b = 153.0 meV
T_s = 120 K
ϕ = <11$\bar{2}$>
0→1
0→0
0→2
I/I_0
0
20
40
60
80
E_z of Incident Beam (meV)

Fig. 3

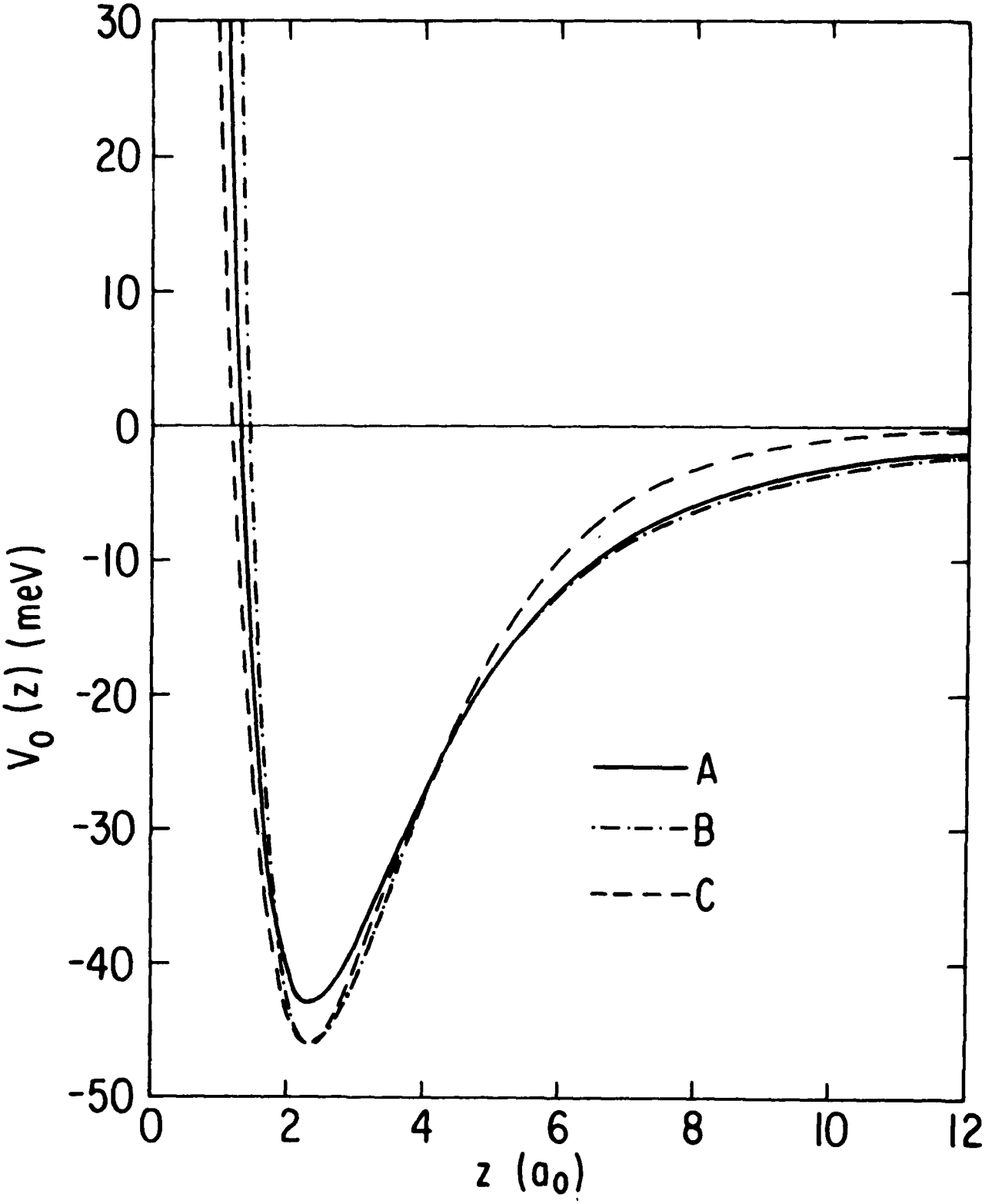

Fig.4

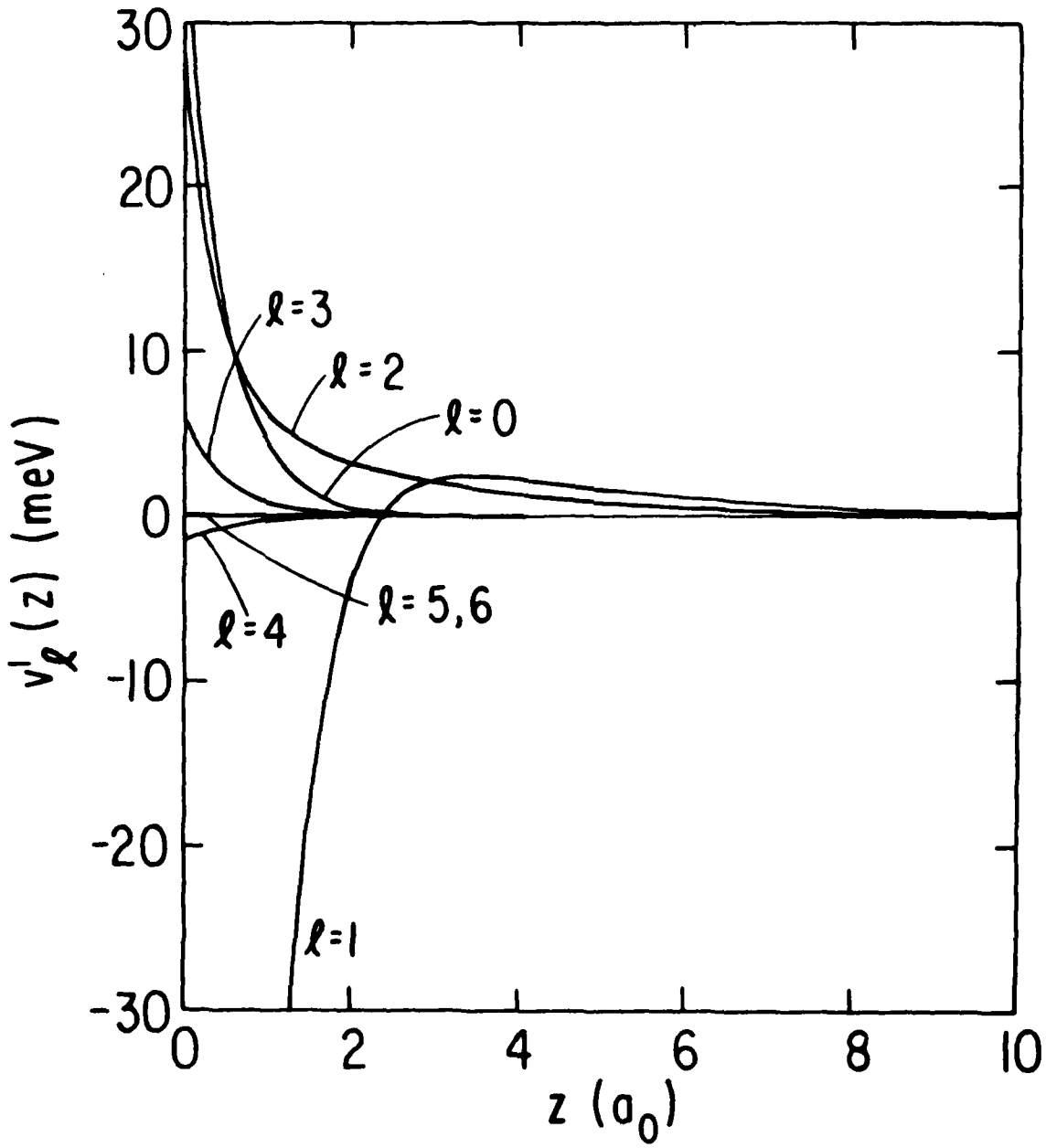

Fig.5

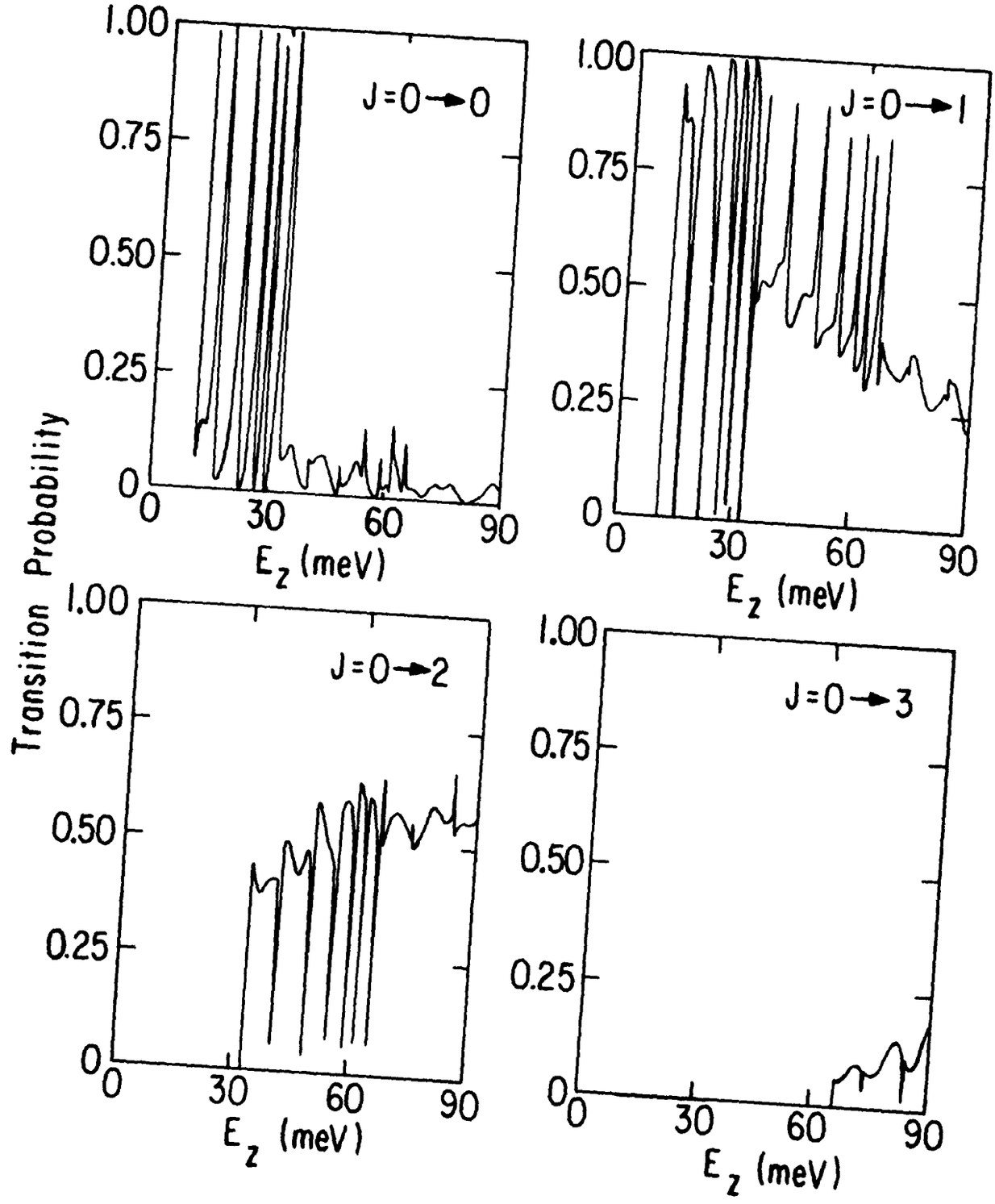
Transition Probability
1.00
0.75
0.50
0.25
0
J=0→0
J=0→1
J=0→2
J=0→3
0
30
60
90
E_z (meV)

Fig.6


DATE
FILMED
9-8